JOURNAL OF PROPULSION AND POWER
Vol. 21, No. 3, May–June 2005

Interactions Between Shock and Acoustic Waves in a Supersonic Inlet Diffuser

Jong Y. Oh,* Fuhua Ma,† Shih-Yang Hsieh,‡ and Vigor Yang§
Pennsylvania State University, University Park, Pennsylvania 16802

The interactions between shock and acoustic waves in a supersonic inlet diffuser are investigated numerically. The model treats the viscous flowfield in an axisymmetric, mixed-compression inlet operating under supercritical conditions. It is solved by means of a finite-volume approach using a four-stage Runge–Kutta scheme for temporal derivatives and the Harten–Yee upwind total-variation-diminishing scheme for spatial terms. Various distinct flow structures, including shock/boundary-layer and shock/shock interactions, are studied under the effects of externally imposed pressure oscillations at the diffuser exit over a wide range of forcing frequencies and amplitudes. As a result of the terminal shock oscillation induced by the impressed disturbances and the cyclic variation of the oblique/normal shock intersection, large vorticity fluctuations are produced in the radial direction. The characteristics of the shock/boundary-layer interactions (such as the size of the separation bubble, the terminal shock configuration, and the vorticity intensity) are also greatly influenced by the acoustic-driven shock oscillation. The overall response of the inlet aerodynamics to acoustic waves can be characterized by the mass-transfer and acoustic-admittance functions at the diffuser exit. Their magnitudes decrease with increasing frequency. A supersonic inlet acts as an effective acoustic damper, absorbing disturbances arising downstream. Severe flow distortion, however, may arise from shock oscillation and subsequently degrade the combustor performance.

Nomenclature

A = cross-sectional area
A_d = acoustic admittance function
a = speed of sound
c_p = constant-pressure specific heat
e_t = specific total energy
f = fluctuation frequency
i = imaginary unit
M = Mach number
Ms = Mach number immediately in front of terminal shock
$\dot{m}$ = mass flow rate
p = pressure
p_b = back pressure (pressure at inlet exit under steady-state calculation)
p_0 = total pressure
R = gas constant
R_c = radius of cowl lip
R_e = radius of inlet exit
R_m = mass response function, identical to $(\dot{m}'/\bar{\dot{m}})/(p'/\bar{p})$
r = radial coordinate
s = entropy
T = temperature
t = time
u = axial velocity
v = radial velocity
x = axial coordinate
x_s = axial position of terminal shock
β = acoustic reflection coefficient
γ = specific heat ratio
Δx_s = shock-displacement amplitude
ε = relative amplitude of imposed pressure fluctuation
ρ = density
Ω = dimensionless frequency, defined by Eq. (19)
ω = radian frequency, $2\pi f$

Subscripts

e = flow properties at inlet exit
1 = flow properties immediately upstream of shock
2 = flow properties immediately downstream of shock

Superscripts

$'$ = fluctuating property
$\bar{}$ = mean property

I. Introduction

An inlet and its interaction with a combustor represent a crucial aspect in the development of ramjets and other supersonic air-breathing engines. The inlet is designed to capture and supply stable airflow at a rate demanded by the combustor and to maintain high pressure recovery and an appropriate stability margin under various engine operating conditions. The overall vehicle performance depends greatly on the energy level and flow quality of the incoming air. A small loss in inlet efficiency translates to a substantial penalty in engine thrust. Furthermore, any change in the inlet flow structure may modify the downstream combustion characteristics and subsequently lead to undesirable behavior, such as flame blowoff and flashback. Thus, matching inlet flow properties to engine requirements is of fundamental importance to designers.[1,2]

The oscillatory behavior of an inlet diffuser flow caused by longitudinal combustion instabilities has often plagued the development of ramjet engines.[3] As a result of unsteady combustion processes, acoustic waves are produced in the combustor and propagate upstream to interact with the shock waves in the inlet. The resultant flow oscillations in the inlet diffuser then either propagate downstream in the form of acoustic waves or are convected downstream with the mean flow in the form of vorticity and entropy waves and

Received 29 March 2004; revision received 13 October 2004; accepted for publication 13 October 2004.

*Graduate Research Assistant, Department of Mechanical Engineering; currently Agency for Defense Development, Republic of Korea.

†Postdoctoral Research Associate, Department of Mechanical Engineering; mafuhua@psu.edu.

‡Research Associate, Department of Mechanical Engineering; currently General Electric Aircraft Engines, Cincinnati, OH.

§Distinguished Professor, Department of Mechanical Engineering. Fellow AIAA.

further reinforce the unsteady motions in the combustor. A feedback loop is, thus, established between the inlet and the combustor. In extreme cases, the shock may be disgorged out of the inlet due to large flow fluctuations, leading to a catastrophic engine failure. A robust inlet design must provide a proper stability margin to accommodate the shock oscillation at the expense of reduced pressure recovery and flow distortion. The present work is an attempt to study the response of inlet aerodynamics to flow disturbances arising from the combustor. Emphasis is placed on the interactions between the shock and acoustic waves in a complicated flowfield typical of an operational supersonic inlet diffuser.

Several experimental investigations have been performed on unsteady inlet diffuser flows with shock waves. In Refs. 4–9, extensive experimental results were reported on transonic and supersonic inlet diffuser flows with pressure oscillations. Various unsteady flow phenomena, such as shock-induced flow separation and shock/acoustic wave interactions under self-excited and forced oscillations, were treated in detail. Gustavsson et al.[10] studied the characteristics of an external-compression supersonic inlet under the effects of pressure disturbances produced by a rotating mechanism at the diffuser exit, to simulate the valve open/close procedures in a pulse detonation engine. Numerical studies were also conducted to reveal details of flowfields by solving two-dimensional conservation equations. Liou and Coakley[11] treated both forced and self-excited oscillations in two-dimensional transonic diffusers with different shock strengths. The work was later extended by Hsieh et al.[12] to provide a closer comparison with experiments.[9] Hsieh et al.[13,14] also examined, in a series of simulations, the response of inlet aerodynamics to various types of pressure disturbances at the diffuser exit, including sinusoidal oscillations over a range of amplitude from 1 to 20% of the mean quantity, single pressure pulses, and monotonically increasing backpressure. Special attention was given to the shock dynamics in a complicated flowfield involving flow separation and acoustic excitation.

Analytical studies were carried out to provide direct insight into the interactions between the shock and acoustic waves in a supersonic inlet. Culick and Rogers[15] treated small-amplitude motions of a normal shock in a one-dimensional flow. The response of the shock wave to imposed acoustic oscillations was characterized with an admittance function for both an inviscid flow and a case in which the influences of flow separation were crudely approximated. Yang and Culick[16] considered the same flow model for finite-amplitude motions using a finite difference scheme with a shock-fitting algorithm. Several different types of disturbances, including large-amplitude periodic oscillations and pulse perturbations, were examined over a broad range of frequencies, along with the effects of liquid droplets on the shock response. Biedron and Adamson[17] characterized the shock wave response to variations in backpressure and wall shape in a two-dimensional supersonic inlet diffuser by means of an asymptotic expansion method. Recently, Robinet and Casalis[18] carried out a one-dimensional stability analysis based on a small-perturbation technique to study self-sustained shock oscillations in several diffusers. Although the frequencies of shock oscillations can be predicted in some cases, their stability approach is limited to the core region where viscous effects are neglected.

Most of the previous studies only treated the flow dynamics downstream of the normal shock in an idealized convergent–divergent channel. The flow evolution upstream of the terminal shock and its influence on the shock structure and response were ignored, giving results remote from the situation in an actual inlet diffuser. This paper presents a more complete analysis of the flowfield in an axisymmetric, mixed-compression supersonic inlet under conditions with and without external forcing. The physical domain of concern includes the entire inlet diffuser, spanning from the freestream to the interface between the inlet and combustor. The formulation accommodates the full conservation equations along with a calibrated two-equation turbulence model and is solved numerically by means of a finite-volume approach. The numerical scheme includes a four-stage Runge–Kutta algorithm for temporal discretization and the Harten–Yee upwind total-variation-diminishing (TVD) method for spatial discretization.

The specific objectives of this work are 1) to investigate the flow development in an entire inlet diffuser under the effects of impressed disturbances at the exit, 2) to examine the details of flow structures in the vicinity of the terminal shock, including the shock/boundary-layer and shock/shock interactions, and 3) to characterize the response of inlet aerodynamics to incident acoustic waves.

II. Theoretical Formulation and Numerical Method

A. Governing Equations

The analysis of the supersonic inlet aerodynamics is based on the Favre-averaged conservation equations of mass, momentum, and energy in the axisymmetric coordinates. In vector notation, this set of equations becomes

$$\frac{\partial \boldsymbol{Q}}{\partial t} + \frac{\partial}{\partial x}(\boldsymbol{E} - \boldsymbol{E}_v) + \frac{\partial}{\partial r}(\boldsymbol{F} - \boldsymbol{F}_v) = \boldsymbol{H} \tag{1}$$

where $\boldsymbol{E}_v$ and $\boldsymbol{F}_v$ are diffusion flux vectors and $\boldsymbol{H}$ is the source-term vector. The conservative variable vector $\boldsymbol{Q}$ and convective flux vectors $\boldsymbol{E}$ and $\boldsymbol{F}$ are defined as

$$\boldsymbol{Q} = r[\rho, \rho u, \rho v, \rho e_t]^T \tag{2}$$

$$\boldsymbol{E} = r\left[\rho u, \rho u^2 + p, \rho uv, (\rho e_t + p)u\right]^T \tag{3}$$

$$\boldsymbol{F} = r\left[\rho v, \rho uv, \rho v^2 + p, (\rho e_t + p)v\right]^T \tag{4}$$

In the preceding equations, standard fluid mechanics notation is used. The pressure p and temperature T are obtained through the equation of state for a perfect gas,

$$p = (\gamma - 1)\left[\rho e_t - \tfrac{1}{2}\rho(u^2 + v^2)\right] \tag{5}$$

$$T = p/(\rho R) \tag{6}$$

The viscosity μ and thermal conductivity λ contain both molecular and turbulent components,

$$\mu = \mu_l + \mu_t, \qquad \lambda = \lambda_l + \lambda_t \tag{7}$$

The laminar component of viscosity μ_l is obtained from Sutherland's law (see Ref. 19)

$$\mu_l/\mu_0 = [(T_0 + S)/(T + S)](T/T_0)^{1.5} \tag{8}$$

where the reference quantities are chosen to be $T_0 = 300$ K, $\mu_0 = 1.8464 \times 10^{-5}$ kg/m · s, and $S = 110$ K for the current problem. The turbulent viscosity μ_t is evaluated using the two-layer model of Rodi because of its ease of implementation and reasonable accuracy in simulating wall-bounded shear layers.[20] The approach combines the standard high Reynolds number k–ε model for the bulk flow region and a one-equation model for the near-wall region. The former solves for turbulent kinetic energy k and its dissipation rate ε directly from the turbulence transport equations. The latter, however, only treats the transport equation for turbulent kinetic energy, with its dissipation rate determined from a prescribed length-scale distribution. The molecular and turbulent thermal conductivities, λ_l and λ_t, are calculated, respectively, from

$$\lambda_l = c_p \mu_l / Pr_l, \qquad \lambda_t = c_p \mu_t / Pr_t \tag{9}$$

where c_p is the specific heat at constant pressure. The Prandtl numbers Pr_l and Pr_t are taken to be 0.73 and 0.9, respectively.

B. Boundary Conditions

The physical domain under consideration is shown schematically in Fig. 1. It consists of the entire internal flow passage in a mixed-compression supersonic inlet diffuser and a freestream region upstream of the inlet. The types of boundaries encountered for the internal and external flowfields are the inflow (AH), outflow (DE), symmetry (AB and CD), wall (BC, EF, and FJ), and far-field (HI and IJ) conditions. Because the inflow is supersonic along the boundary AH, the flow variables are fixed at their corresponding freestream

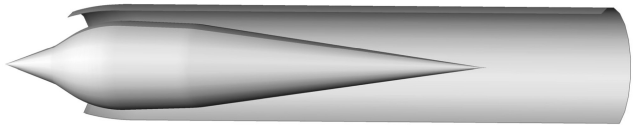

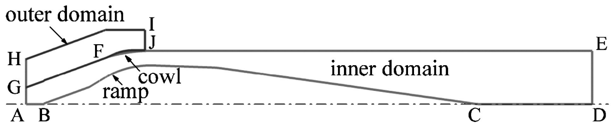

Fig. 1 Schematic of mixed-compression supersonic inlet and computational domain.

values. At the exit boundary of the inlet, DE, a constant backpressure is specified, and the other flow variables are extrapolated from the interior for steady-state calculations. For cases involving flow oscillations, a sinusoidal pressure fluctuation is applied at the diffuser exit and the nonreflective boundary conditions proposed by Watson and Myers[21] is implemented. The radial velocity and the normal gradients of the axial velocity, pressure, and temperature at the centerline are set to zero due to flow symmetry. The no-slip boundary condition and zero normal gradients of the pressure and temperature are enforced along the wall. Finally, the flow variables at the far-field boundary are extrapolated from the interior along the characteristic lines, based on the solution of a simple wave,[22] to avoid shock reflections.

C. Numerical Method and Model Validation

The governing equations and their associated boundary conditions as just outlined are solved numerically by means of a density-based, finite-volume methodology. Temporal discretization is obtained using a four-stage Runge–Kutta integration method. The spatial discretization employs an upwind TVD scheme developed by Harten[23] and Yee[24] in generalized coordinates for convective terms and a second-order central-differencing method for diffusion terms. Specific details of the numerical algorithm may be found in Ref. 25.

The overall approach has been validated against a variety of flow problems to assess its accuracy. One of the validation cases involves a supersonic flow over a cone with a half-angle of 20 deg. The freestream Mach number and pressure are 2.1 and 0.29 atm, respectively, under which conditions a conical oblique shock is attached to the cone vertex. The exact solution for this case is available by solving the ordinary differential equation derived by Taylor and Maccoll[26] and it is compared with the present calculation. The calculated Mach number and pressure distributions with respect to the angle of the ray from the cone vertex are in good agreement with the exact solutions.[25] The turbulence model is tested for the turbulent boundary layer on a flat plate. The calculated velocity profiles agree very well with the results from the direct numerical simulations for $Re_\theta = 1.41 \times 10^3$ (Ref. 27). A more detailed discussion of the model validation is given in Ref. 25.

III. Results and Discussion

After validation, the analysis is applied to the flowfield in an axisymmetric, mixed-compression supersonic inlet under conditions with and without external forcing at the diffuser exit. Figure 2 shows the inlet configuration treated in the current study, optimized for a flight altitude of 9.3 km and a Mach number of 2.1. The front part of the centerbody involves a double cone with half-angles of 20 and 31.25 deg. The cowl radius is $R_c = 3.4$ cm. The throat is located at about $x = 7.87$ cm, with a radial size of 1.05 cm. The freestream static pressure and temperature are 0.29 atm and 228 K, respectively, and the corresponding total pressure and temperature are 2.65 atm and 428 K. The Reynolds number based on the cowl radius and freestream conditions is 6.54×10^5.

The computational domain shown in Fig. 1 comprises an internal flow region, that is, the inner domain, containing most of the essential flow structure, and an external flow region, that is, the outer domain, which becomes important when flow spillage over

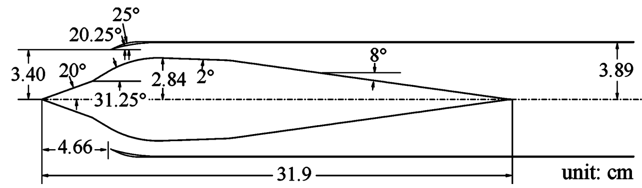

Fig. 2 Configuration of mixed-compression supersonic inlet.

the cowl lip occurs at subcritical operating conditions. The numerical grid system consists of 601×101 points for the inner domain and 201×81 points for the outer domain. The grids are stretched toward the walls to resolve rapid flow variations in the boundary layers. A grid-independence study was performed by increasing the grid numbers by 50% in the axial direction and 25% in the radial direction. Results for the steady-state flowfields obtained from these two grids are almost identical. The relative difference in terms of the terminal shock position is less than 1%. A stricter grid-independence study may be conducted based on the Richardson extrapolation (see Ref. 28).

A. Steady-State Flowfield

The steady-state flowfield is first studied to establish a fundamental understanding of the flow structure and to provide a basis for the examination of the response of the inlet flow to downstream disturbances. Figure 3 shows the Mach number, pressure, and vorticity contours for two different backpressures ($p_b = 2.1$ and 2.2 atm) under steady-state operating conditions. The two leading conical shocks generated by the double-cone centerbody compress the airflow externally, merge slightly above the cowl lip, and form a strong oblique shock extending into the external-flow region. In addition, a shock stemming from the cowl inner surface continues downstream, hitting and reflecting from the cowl and centerbody walls and finally leading to a terminal normal shock. The flow in this region undergoes a series of compression and expansion processes, being compressed by reflected shocks and expanded by expansion waves, as clearly illustrated by the enlarged Mach number contours in Fig. 4. The wavy distributions of the Mach number and pressure along the middle line of the inlet duct, as shown in Fig. 5 for the case of $p_b = 2.1$ atm, also demonstrate this feature. The flow finally becomes subsonic after passing through the terminal shock. During this process, the flow direction, which is originally deflected away by the leading shocks, is adjusted back to the axial direction. The present design allows the inlet to recover a high percentage of the freestream total pressure by decelerating the airflow through the shock train. The total-pressure recovery coefficients are 84% for the case of $p_b = 2.1$ atm and 88% for $p_b = 2.2$ atm, and the Mach numbers immediately in front of the terminal shocks are 1.42 and 1.32, respectively. The terminal shock is located in the divergent section ($x_s = 9.7$ cm) for $p_b = 2.1$ atm. This situation corresponds to a supercritical condition. The shock is shifted upstream to a position near the throat ($x_s = 7.9$ cm) for $p_b = 2.2$ atm, corresponding to a near-critical condition.

Because of viscous effects, boundary layers exist near both the cowl and centerbody walls. Their interactions with shock waves play an important role in dictating the inlet flow structure. Figure 6 shows the closeup view of the flowfield near the terminal shock. The boundary layer prohibits an abrupt change in pressure across the shock near the wall because the flow in the inner part of the boundary layer remains subsonic. Part of the pressure rise across the shock is transmitted upstream through this subsonic region and causes the streamlines to diverge. The boundary layer thickens and may be separated from the wall if the pressure rise is sufficiently large. As a consequence, the terminal shock is no longer one dimensional. An oblique shock forms due to the rapid growth of the boundary-layer displacement and runs into the terminal shock. If the flow deflection is sufficiently large after passing the leading oblique shock, a rear oblique shock emerges to form a λ structure.[1,29] The abrupt thickening of the boundary layer downstream of the normal shock reduces the effective flow passage area and subsequently accelerates the subsonic flow behind the shock. The steep pressure decrease (or Mach number increase) immediately downstream of

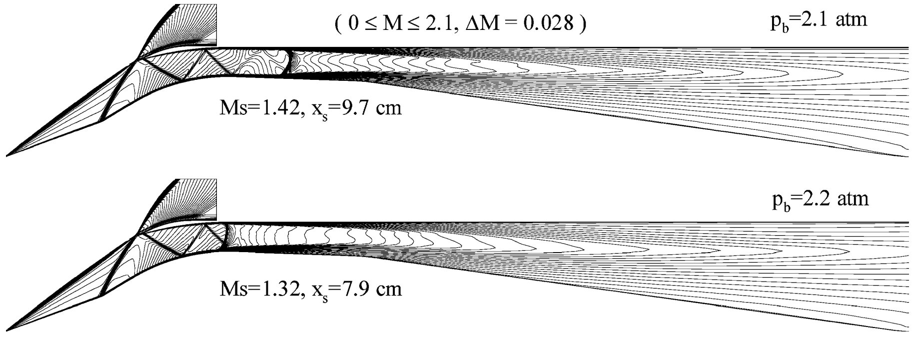

a) Mach number

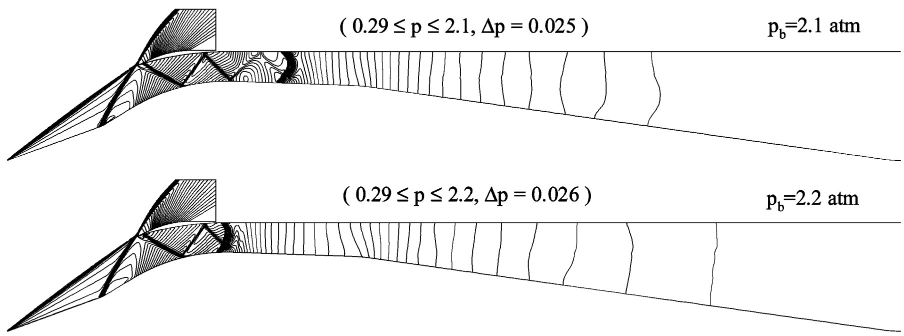

b) Pressure contours

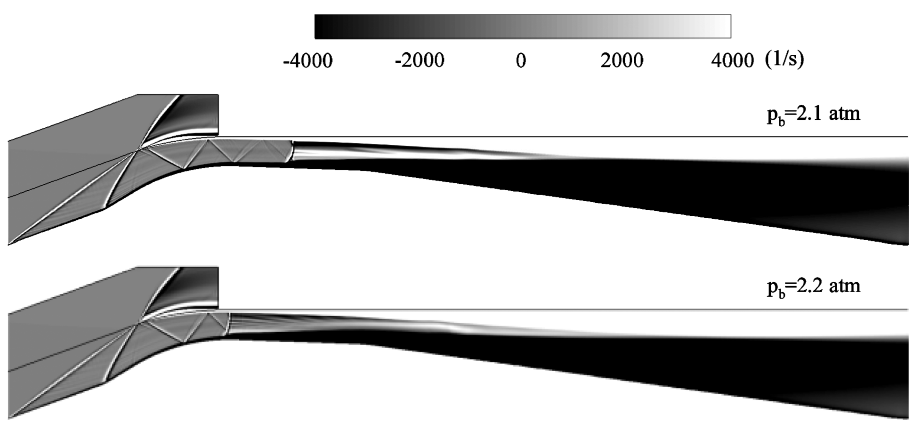

c) Vorticity contours

Fig. 3 Mach number, pressure, and vorticity contours with backpressures of 2.1 and 2.2 atm under steady-state conditions.

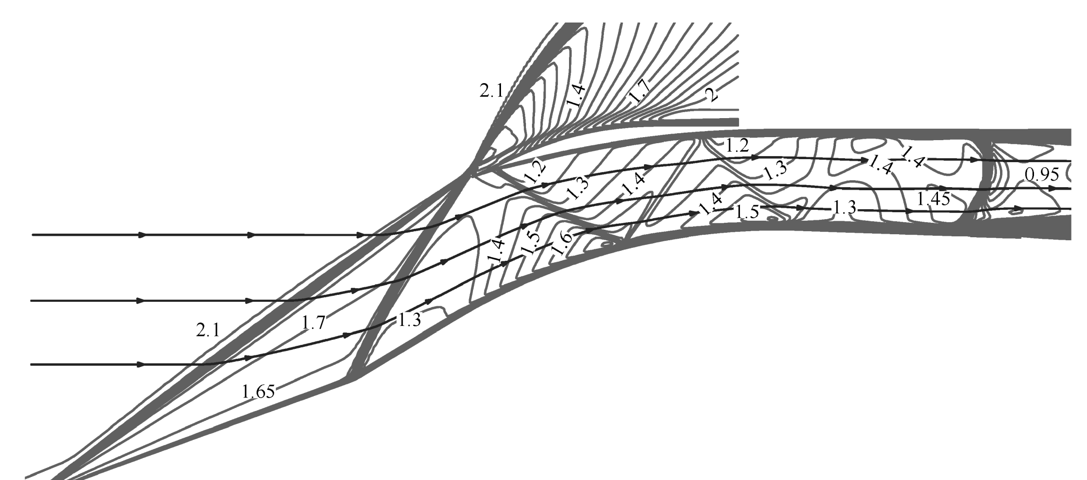

Fig. 4 Closeup of Mach number contours and streamlines, $p_b = 2.1$ atm.

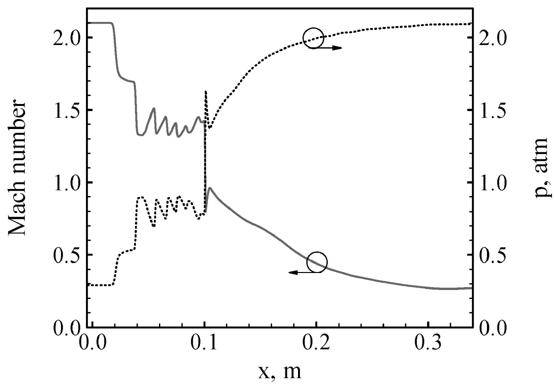

Fig. 5 Mach number and pressure distributions along midline of inlet diffuser under steady-state condition, $p_b =$ 2.1 atm.

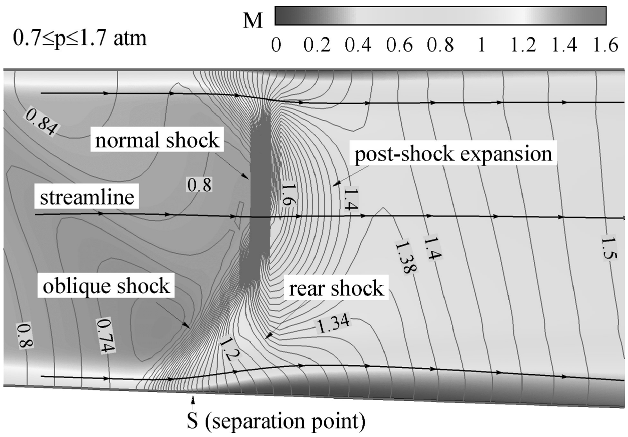

Fig. 6 Closeup of Mach number (flood) and pressure (line) fields near terminal shock, $p_b = 2.1$ atm.

the terminal shock in the core flow region, as shown in Fig. 5, is attributed to this post-shock expansion effect.

Because the flow passing through the normal shock is slower than that through the oblique shocks, two vortex sheets emanate from the upper and lower shock bifurcation points and are convected downstream. This phenomenon is clearly seen in the vorticity contours in Fig. 3. Another vortex sheet develops due to the different compression history of the flow immediately upstream of the terminal shock: some of the flow passes through the final reflected oblique shock and some of it does not. Note, however, that much of the vorticity downstream of the terminal shock is generated in the wall boundary layers. The vorticity scale in Fig. 3 was carefully chosen to elucidate the strength of the vorticity in the core flow region. The vorticity magnitude inside the boundary layers is, of course, much larger than that in the core flow region.

B. Response of Inlet Flow to Downstream Disturbance

To characterize the response of the inlet aerodynamics to disturbances arising downstream, sinusoidal pressure oscillations are imposed at the exit plane, simulating acoustic motions induced by the unsteady combustion in the chamber,

$$p'_e = \varepsilon p_b \sin(\omega t) \tag{10}$$

where ε is the relative amplitude of the oscillation. The study considers a wide range of oscillation amplitudes, with $0 \le \varepsilon \le 10\%$, and frequencies, with $250 \le f \le 4000$ Hz. The baseline conditions include $\varepsilon = 0.05$ and $f = 500$ Hz. For each case, calculations are conducted over an extended time period to ensure that the flowfield has reached its steady oscillation.

Unsteady Flowfield

Figure 7 shows the temporal evolution of the pressure distributions along the cowl and centerbody walls and the midline over one cycle of oscillation for the baseline case. The corresponding Mach number contours near the terminal shock are also presented to reveal the detailed flow structure. In Fig. 7, S is the flow separation point on the centerbody wall, PP the pressure pulse, and Ms the Mach number in front of the terminal shock. Each oscillation cycle begins when the terminal shock is located at its time-averaged position. As the shock moves upstream, its shape and strength vary in response to the change in the local flowfield and the intersection with the upstream oblique shocks. Because it is the relative Mach number that determines the strength of a shock, the terminal shock may either strengthen or weaken as it travels upstream, in spite of the decrease in the flow velocity upstream of the shock (Fig. 4). This is in contrast to the previous observation by Hsieh et al.[14] that the shock becomes weaker as it moves upstream. The discrepancy may be attributed to the smoother diffuser contour near the terminal shock in the present study. As a result, the variation of the local flow velocity is smaller, and the shock velocity becomes higher and may reach 50 m/s for the baseline case. The resultant flow Mach number relative to the terminal shock, thus, increases during its propagation. The terminal shock reverses its direction after reaching the farthest upstream position at the time of about $\omega t = \pi$. Similarly, as it travels downstream, the strength first increases and then decreases when the increase in the shock velocity exceeds that in the local flow velocity. At $\omega t = 7\pi/6$, the terminal shock becomes a Mach stem attached to the cowl wall and, thus, cannot be detected in the core region. As the shock velocity further increases, the terminal shock disappears and degenerates to a pressure pulse. On the other hand, a strong adverse pressure gradient arising from the impressed disturbance gradually develops downstream and eventually steepens into a secondary shock. This shock continuously increases its strength as it moves upstream and finally merges into the primary shock (or pressure pulse) to form a stronger shock. The first dense-line region (denoted PP) in the Mach number snapshot at $\omega t = 3\pi/2$ is in fact a pressure pulse rather than a shock, whereas the second dense-line region corresponds to the weak secondary shock. Figure 7 also shows that the terminal shock induces boundary-layer separation once its strength reaches a threshold value with Ms around 1.4. The two separation points at $\omega t = 5\pi/3$ (S_1 and S_2) result from the terminal shock and the adverse pressure gradient caused by the impressed acoustic wave and divergence of the cross-sectional area, respectively.

Figure 8 shows the temporal evolution of the fluctuating vorticity field (obtained by subtracting the steady-state quantity from the instantaneous value) within one cycle of oscillation for the baseline case. The continuous movement of the terminal shock and its subsequent influence on the near-wall flowfields give rise to large vorticity fluctuations. The vortex sheets, originating from the intersections between the terminal and oblique shocks, also change their distributions and strengths periodically in both the axial and radial directions as the terminal shock oscillates. The resultant vorticity fluctuation is complex and multidimensional.

Shock Oscillation

Figure 9 shows the time histories of the instantaneous terminal shock location for different forcing frequencies and amplitudes. The shock position is determined by searching along the midline for the point at which the flow Mach number equals unity. At $t = 0$, a periodic pressure oscillation is imposed at the diffuser exit. The shock begins to respond after a short duration, when the disturbance arrives. The shock then executes a sinusoidal motion around its mean position for small-amplitude fluctuations. The oscillation of the shock displacement in general increases with increasing amplitude and decreasing frequency of the impressed disturbance, a phenomenon which was well established in previous studies.[15,16] As the disturbance becomes larger, that is, $\varepsilon = 5\%$, many nonlinear phenomena emerge, as elucidated in Fig. 9b. The shock moves faster downstream than upstream, and its oscillation is no longer sinusoidal. In addition, a secondary shock forms and the primary shock disappears sometime within the cycle (Fig. 7). Further increasing the oscillation amplitude to ε = 10% causes the terminal shock to travel continuously upstream and eventually be disgorged out of the inlet.

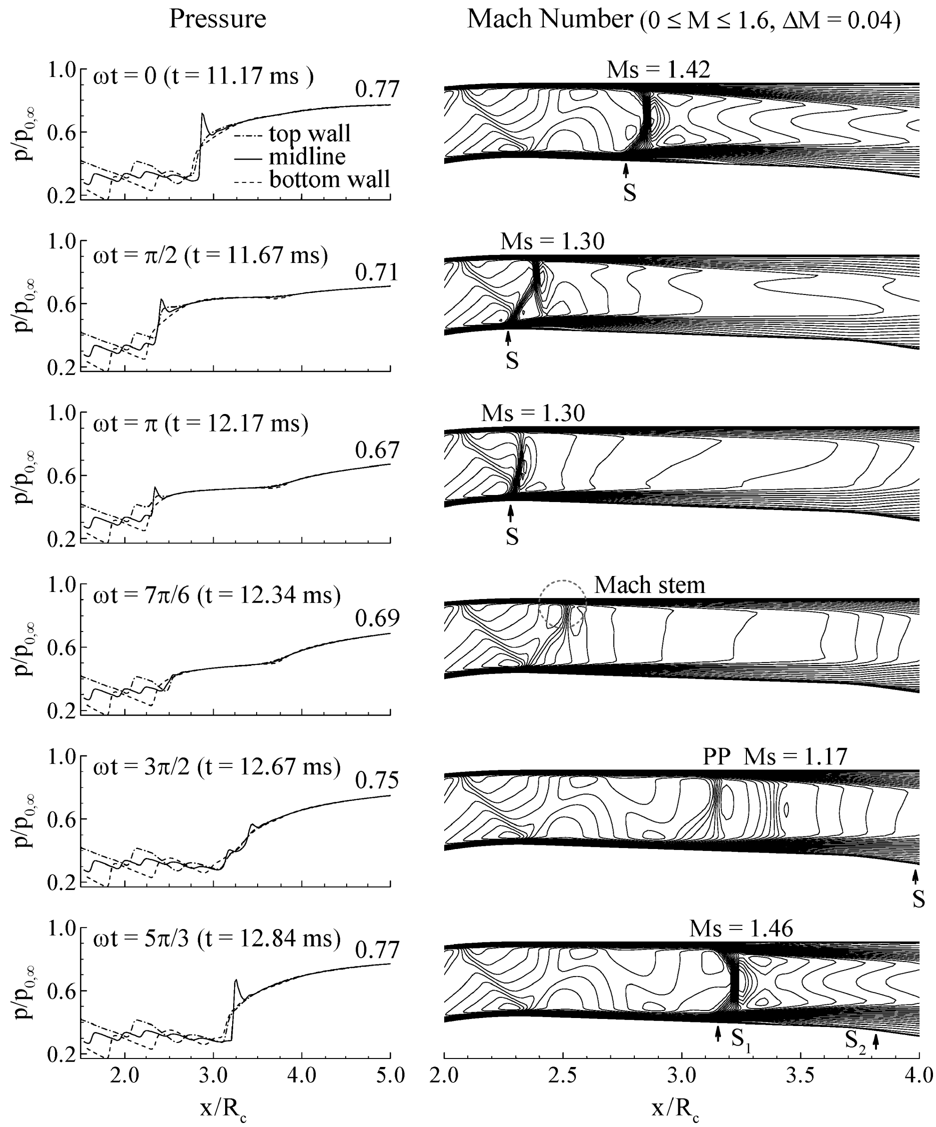

Fig. 7 Temporal evolution of pressure distributions along walls and midline of inlet and Mach number contours within one cycle of oscillation, $\varepsilon = 0.05$ and $f = 500$ Hz.

Figure 10 shows the effect of forcing frequency on the excursion of the terminal shock for two different amplitudes, $\varepsilon = 1\%$ and 5%. The shock displacement decreases with increasing frequency. For small-amplitude fluctuations ($\varepsilon = 1\%$), the farthest upstream and downstream positions are nearly symmetric with respect to the steady-state position. The oscillation amplitudes of the shock movement can be predicted using the following analytic formula, derived by Culick and Rogers,[15] which treats the response of a normal shock wave to downstream disturbances in an inviscid flowfield:

$$\Delta x_s = \frac{\Delta p}{\bar{p}_1} \Bigg/ \sqrt{\left[\frac{2\pi f}{\bar{a}_1} \cdot \frac{4\gamma \bar{M}_1}{\gamma + 1}\right]^2 + \left[\left(\frac{1}{A}\frac{\mathrm{d}A}{\mathrm{d}x}\right)_s g(\bar{M}_1)\right]^2} \qquad (11)$$

where $\bar{p}_1$, $\bar{a}_1$, and $\bar{M}_1$ are the mean pressure, sound speed, and Mach number immediately upstream of the shock and Δp is the pressure-oscillation amplitude behind the shock. The subscript s represents the value at the normal shock, and

$$g(\bar{M}_1) = \left[(\gamma^2 + 1)\bar{M}_1^2 + (\gamma - 1)\right] \big/ [(\gamma + 1)^2/2\gamma] \qquad (12)$$

Figure 11 shows good agreement between the analytical prediction and the present numerical result. The situation with finite amplitude oscillations, however, becomes considerably different. The various nonlinear and multidimensional effects involved in the interactions between the acoustic and shock waves in a viscous environment prohibit the use of a simple one-dimensional model to predict the shock response.

Flow Properties at Exit Plane

The flow properties at the diffuser exit characterize the coupling between the inlet and the combustor of an engine and must be carefully studied. Figure 12 shows the fluctuations of the axial velocity and total pressure at different radial positions at the trailing edge of the centerbody over one cycle of oscillation for the baseline case ($\varepsilon = 5\%$ and $f = 500$ Hz). These quantities are normalized with respect to the time–mean speed of sound and exit pressure, respectively. The velocity oscillations are approximately sinusoidal except in the region near the upper wall, where the vortex sheets extending from the intersection between the oblique and terminal shocks take effect. The fluctuation amplitude varies in the radial direction, from less than 3.6% in the upper part to about 6% at the midpoint. Based on one-dimensional acoustic theory, the normalized velocity fluctuation has the same amplitude as the normalized pressure fluctuation for a traveling wave in an inviscid flowfield. The deviation of the present result from that predicted from simple acoustic theory arises from the vortical fluctuations in the viscous layers and the oscillatory intersection between the oblique and terminal shock waves. The reflection of the incident disturbance from the centerbody walls also contributes to such a nonuniform distribution of flow variations in the radial direction.

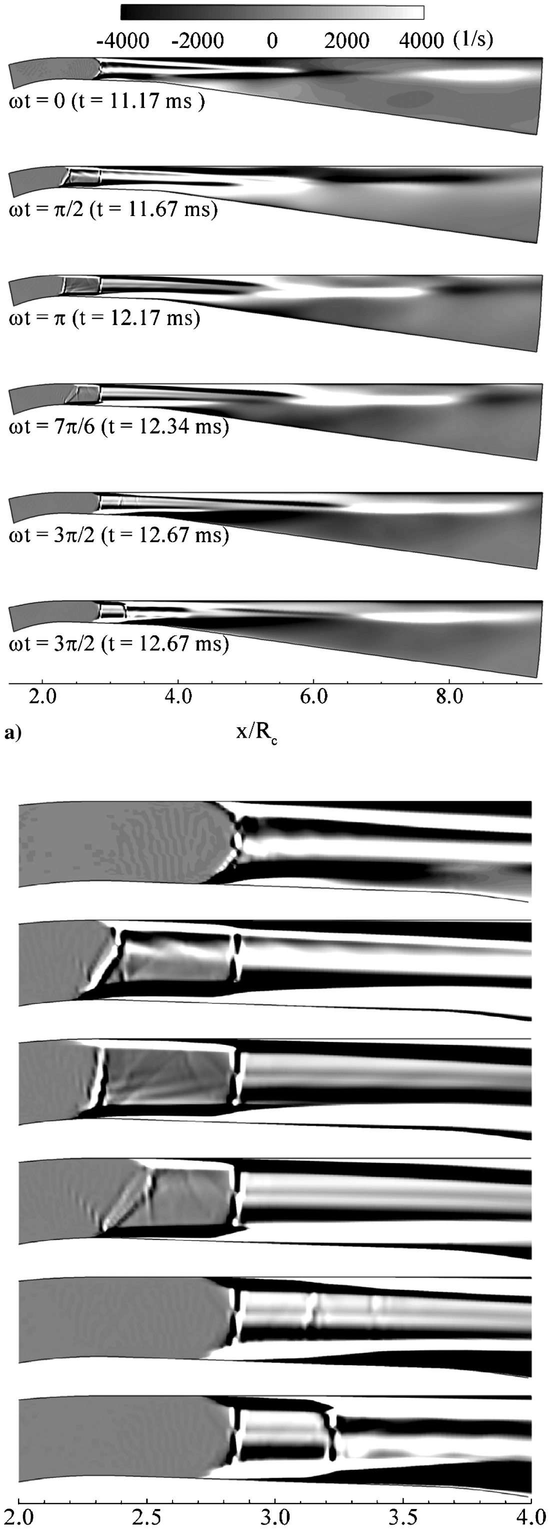

Fig. 8 Fluctuating vorticity field within one cycle of oscillation near terminal shock, $\varepsilon = 0.05$ and $f =$ 500 Hz: a) global view and b) closeup.

The total pressure fluctuation exhibits a sinusoidal behavior. The phase difference between the velocity and pressure fluctuation is about 180 deg. When it is considered that

$$p_0 = p[1 + (\gamma - 1)/2 \cdot u^2/a^2]^{\gamma/(\gamma - 1)} \tag{13}$$

and that the speed of sound a is almost constant, the relative amplitude of the total pressure fluctuation is smaller than that of the

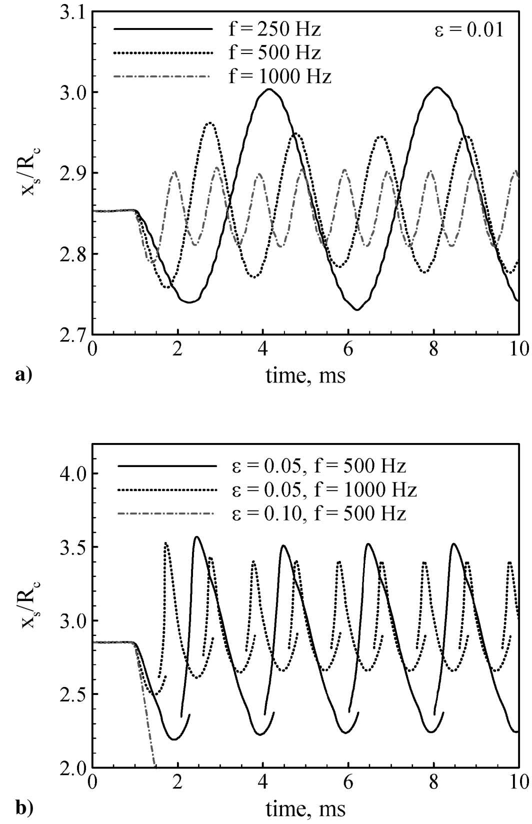

Fig. 9 Time histories of terminal shock locations for different forcing frequencies: a) small-amplitude oscillations and b) finite-amplitude oscillations.

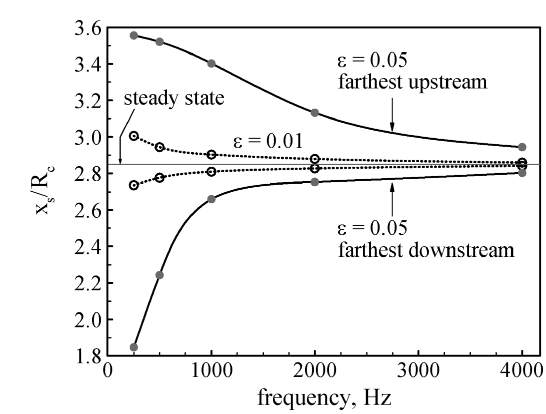

Fig. 10 Effect of forcing frequency and amplitude on terminal shock movement.

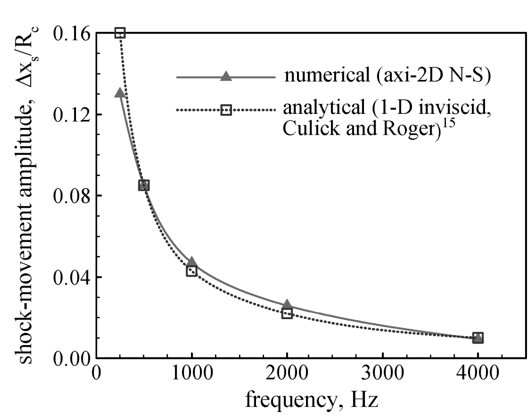

Fig. 11 Comparison of oscillation amplitude of terminal shock movement between numerical and analytical results, $\varepsilon =$ 0.01.

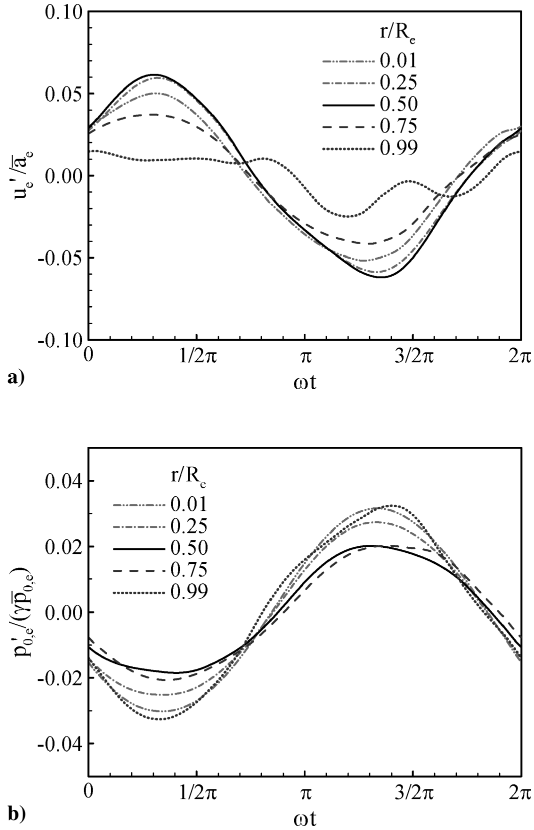

Fig. 12 Variations over time at trailing edge of centerbody over one cycle of oscillation, $\varepsilon = 0.05$ and $f = 500$ Hz: a) fluctuating axial velocity and b) total pressure at five different radial positions.

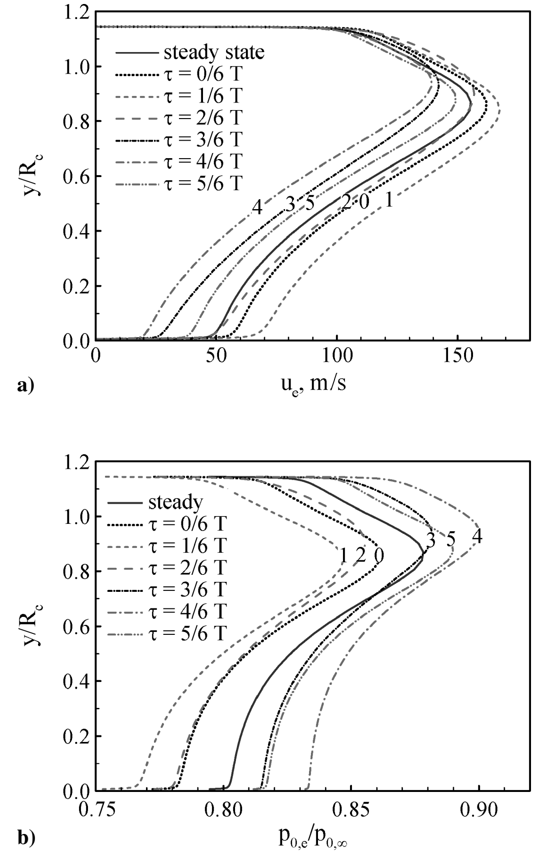

Fig. 13 Temporal evolution of radial distributions within one cycle of oscillation, $\varepsilon = 0.05$ and $f = 500$ Hz: a) axial velocity and b) total pressure at trailing edge of centerbody.

pressure due to the out-of-phase relationship between the fluctuating velocity and pressure. The normalized fluctuation amplitude of the total pressure, $p'_{0,e}/\gamma\,\bar{p}_{0,e}$, is 1.8% at the midpoint, which is half of the corresponding pressure fluctuation.

One of the inlet design requirements is to provide a uniform distribution of the discharge velocity at the exit plane, to achieve stable combustion and prevent the occurrence of flame blowoff and flashback. It is, thus, important to examine the effect of acoustic disturbances on the discharge profiles. Figure 13 shows the temporal evolution of the radial distributions of the axial velocity and total pressure at the trailing edge of the centerbody during one cycle of oscillation for the baseline case. The axial velocity increases from the bottom wall, reaches its maximum above the midpoint, and then decreases toward the upper wall. The flowfield is severely distorted due to the merging of the two boundary layers originating from the top and bottom roots of the terminal shock (Fig. 3). The impressed disturbances, although they do cause flow oscillations, exert little influence on the radial distributions of the flow properties at the exit plane.

Airflow matching is another important issue of inlet design. Engine performance may degrade rapidly if the captured flow does not meet the requirement for efficient and stable combustion.[2] Figure 14 shows the transfer function between the exit mass flow rate and the impressed pressure fluctuation. The amplitude varies from 1.6 to about 2.1, depending on the oscillation frequency and amplitude. A simple mass balance relates the fluctuating mass flow rate to the local velocity, pressure, and entropy fluctuations as follows:

$$\dot{m}'_e/\bar{\dot{m}}_e = \rho'_e/\bar{\rho}_e + u'_e/\bar{u}_e = p'_e/\gamma\,\bar{p}_e - s'_e/c_p + u'_e/\bar{u}_e \qquad (14)$$

where the subscript e denotes the bulk flow quantity at the exit. The mass response function is then expressed as

$$R_m \equiv \frac{\dot{m}'_e/\bar{\dot{m}}_e}{p'_e/\bar{p}_e} = \frac{1}{\gamma}\left(1 + \frac{u'_e/\bar{a}_e}{p'_e/\gamma\,\bar{p}_e}\cdot\frac{\bar{a}_e}{\bar{u}_e} - \frac{s'_e/c_p}{p'_e/\gamma\,\bar{p}_e}\right) \qquad (15)$$

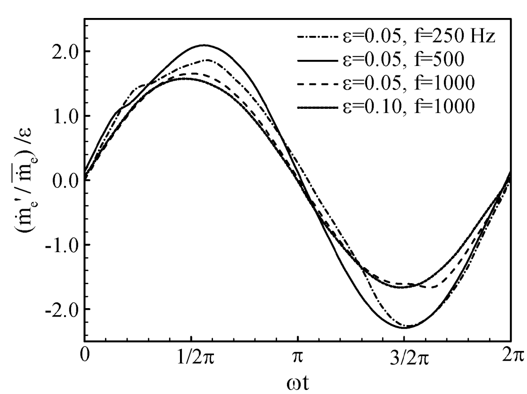

Fig. 14 Temporal evolution of mass flow fluctuations at trailing edge of centerbody within one cycle of oscillation for different forcing amplitudes and frequencies.

If we ignore the entropy fluctuation arising from the shock oscillation and the acoustic wave reflected from the shock,

$$(u'_e/\bar{a}_e)/(p'_e/\gamma\,\bar{p}_e) = -1 \qquad (16)$$

the mass response function can be directly related to the imposed pressure disturbance,

$$R_m \equiv (1 - \bar{a}_e/\bar{u}_e)/\gamma \qquad (17)$$

Substituting $\bar{a}_e = 408$ m/s and $\bar{u}_e = 127$ m/s into Eq. (17) gives an amplitude of 1.58, which represents a major part of the overall mass response. In addition to the imposed acoustic disturbance, the mass flow fluctuation contains a contribution from the shock oscillation. Even for a fixed mass flow rate upstream of the shock, an oscillation will occur in the downstream region due to the shock motion. Such

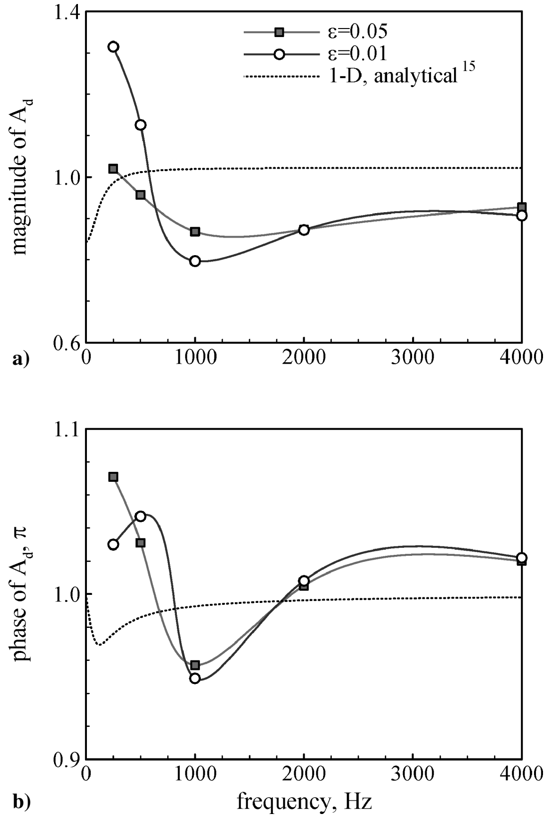

Fig. 15 Acoustic-admittance function at exit plane as function of frequency: a) magnitude and b) phase angle.

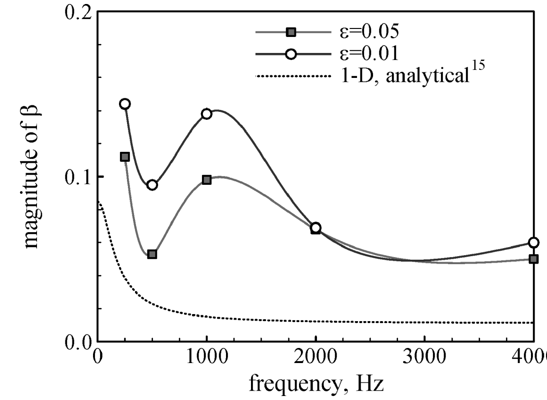

Fig. 16 Magnitude of acoustic-reflection coefficient at exit plane as function of frequency.

a shock-induced oscillation can be estimated by the product of the shock velocity, cross-sectional area, and density difference across the shock.[16]

The overall response of the inlet aerodynamics can be characterized using the acoustic admittance function and reflection coefficient at the exit plane. Results can be used as the upstream boundary conditions to investigate the stability characteristics of the combustor in the downstream direction. Figure 15 shows the magnitude and phase of the admittance function, calculated based on the fluctuations of the pressure and mass-averaged axial velocity at the exit plane. Also included is the admittance function of a normal shock in response to downstream disturbances, derived analytically by Culick and Rogers[15] for an inviscid flow. The analytical formula, after correcting a typographical error in Ref. 15, is expressed as

$$A_d \equiv \frac{u'/\bar{a}_2}{p'/\gamma\,\bar{p}_2} = \left(-\frac{2}{\gamma+1}\cdot\frac{\bar{M}_1^2+1}{\bar{M}_1^2}\Omega i + \frac{2\gamma\bar{M}_2}{\gamma+1}\right)\Bigg/\left[\frac{4\bar{M}_1}{\gamma+1}\left(\frac{\bar{p}_1}{\bar{p}_2}\frac{\bar{a}_2}{\bar{a}_1}\right)\Omega i - \frac{\gamma^2+1}{\gamma^2+\gamma}\cdot\left(\bar{M}_1^2+\frac{\gamma-1}{\gamma^2+1}\right)\left(\bar{M}_1^2-\frac{\gamma-1}{2\gamma}\right)^{-1}\right] \tag{18}$$

where $\bar{p}$, $\bar{a}$, and $\bar{M}$ are the mean pressure, speed of speed, and Mach number, respectively. The subscripts 1 and 2 indicate the quantities immediately upstream and downstream of the shock, respectively. The dimensionless frequency Ω is defined as

$$\Omega = \frac{2\pi f}{\bar{a}_2}\left(\frac{1}{A}\frac{\mathrm{d}A}{\mathrm{d}x}\right)_s^{-1} \tag{19}$$

with subscript s representing the value at the normal shock. The acoustic admittance function varies considerably in the low-frequency region and levels off at high frequencies, as in the analytical results. The discrepancy between the one-dimensional analytical and present numerical results mainly arises from the reflection of the incident acoustic wave from the centerbody wall and the nonlinear behavior of the shock oscillation as well as its induced vorticity oscillation. The amplitude of the imposed pressure disturbance also plays a significant role. The phase angle of the admittance function remains close to π, revealing the predominance of the upstream-traveling wave in the flowfield.[15,16]

Figure 16 shows the magnitude of the acoustic reflection coefficient at the exit plane, defined as the ratio of the magnitude between the reflected and incident waves. The reflection coefficient can be related to the admittance function as follows, based on simple acoustic theory:

$$\beta = (1 + A_d)/(1 - A_d) \tag{20}$$

It has been well established that the magnitude of the reflection coefficient of a normal shock decreases with increasing frequency.[15] Also, the shock acts as an effective acoustic damper, absorbing acoustic disturbances arising from the downstream region. The shock reflection coefficient is in general small, and the acoustic field in a supersonic inlet is dominated by wave motions traveling upstream. The present analysis corroborates the analytical prediction developed in Ref. 15, in spite of the small differences due to the multidimensional effects and reflection from the centerbody wall, which were not taken into account in the analytical theory.

IV. Summary

The interactions between shock and acoustic waves were numerically investigated for a viscous flowfield in an axisymmetric, mixed-compression supersonic inlet diffuser under supercritical operation. The response of inlet aerodynamics to imposed pressure disturbances at the exit were examined over a wide range of forcing frequencies (250 ∼ 4000 Hz) and amplitudes (1 ∼ 10%). Important phenomena of concern include temporal and spatial variations of mass flow rate, total pressure, and flow distribution, as well as shock displacement. In general, the acoustic response of the terminal shock increases with increasing amplitude of the imposed disturbance, but decreases with frequency. As a result of the shock oscillation, large vorticity fluctuations are produced in the radial direction. The overall response of the inlet aerodynamics was characterized by the acoustic admittance function and reflection coefficient at the diffuser exit. Results demonstrate that a supersonic inlet under supercritical operation acts as an effective acoustic damper absorbing disturbances arising downstream.

Acknowledgment

This work represents a part of the results obtained from a research program supported by the Chung-Shan Institute of Science and Technology, Taiwan, Republic of China.

References

[1]Seddon, J., and Goldsmith, E. L., *Intake Aerodynamics*, 2nd ed., AIAA Education Series, AIAA, Reston, VA, 1999, pp. 56–61.

[2]Yang, V., and Cappuccio, M., *Supersonic Inlet Design for Missiles*, Research Rept., Dept. of Mechanical Engineering, Pennsylvania State Univ., University Park, PA, Jan. 1991.

[3]Clark, W. J., "Experimental Investigation of Pressure Oscillations in a Side Dump Ramjet Combustor," *Journal of Spacecraft*, Vol. 19, No. 1, 1982, pp. 47–53.

[4]Chen, C. P., Sajben, M., and Kroutil, J. C., "Shock-Wave Oscillations in a Transonic Diffuser Flow," *AIAA Journal*, Vol. 17, No. 10, 1979, pp. 1076–1083.

[5]Bogar, T. J., Sajben, M., and Kroutil, J. C., "Characteristic Frequencies of Transonic Diffuser Flow Oscillations," *AIAA Journal*, Vol. 21, No. 9, 1983, pp. 1232–1240.

[6]Salmon, J. T., Bogar, T. J., and Sajben, M., "Laser Doppler Velocimeter Measurements in Unsteady, Separated, Transonic Diffuser Flows," *AIAA Journal*, Vol. 21, No. 12, 1983, pp. 1690–1697.

[7]Sajben, M., Bogar, T. J., and Kroutil, J. C., "Forced Oscillation Experiments in Supercritical Diffuser Flows," *AIAA Journal*, Vol. 22, No. 4, 1984, pp. 465–474.

[8]Bogar, T. J., Sajben, M., and Kroutil, J. C., "Response of a Supersonic Inlet to Downstream Perturbations," *Journal of Propulsion and Power*, Vol. 1, No. 2, 1985, pp. 118–125.

[9]Bogar, T. J., "Structure of Self-Excited Oscillations in Transonic Diffuser Flows," *AIAA Journal*, Vol. 24, No. 1, 1986, pp. 54–61.

[10]Gustavsson, J., Nori, V., and Segal, C., "Inlet/Engine Interactions in an Axisymmetric Pulse Detonation Engine System," *Journal of Propulsion and Power*, Vol. 19, No. 2, 2003, pp. 282–286.

[11]Liou, M. S., and Coakley, T. J., "Numerical Simulations of Unsteady Transonic Flow in Diffusers," *AIAA Journal*, Vol. 22, No. 8, 1984, pp. 1139–1145.

[12]Hsieh, T., Bogar, T. J., and Coakley, T. J., "Numerical Simulation and Comparison with Experiment for Self-Excited Oscillations in a Diffuser Flow," *AIAA Journal*, Vol. 25, No. 7, 1987, pp. 936–943.

[13]Hsieh, T., Wardlaw, A. B., Jr., Collins, P., and Coakley, T. J., "Numerical Investigation of Unsteady Inlet Flowfields," *AIAA Journal*, Vol. 25, No. 1, 1987, pp. 75–81.

[14]Hsieh, T., Wardlaw, A. B., Jr., and Coakley, T. J., "Ramjet Diffuser Flowfield Response to Large-Amplitude Combustor Pressure Oscillations," *Journal of Propulsion and Power*, Vol. 3, No. 5, 1987, pp. 472–477.

[15]Culick, F. E. C., and Rogers, T., "The Response of Normal Shocks in Diffusers," *AIAA Journal*, Vol. 21, No. 1, 1983, pp. 1382–1390.

[16]Yang, V., and Culick, F. E. C., "Analysis of Unsteady Inviscid Diffuser Flow with a Shock Wave," *Journal of Propulsion and Power*, Vol. 1, No. 3, 1985, pp. 222–228.

[17]Biedron, R. T., and Adamson, T. C., Jr., "Unsteady Flow in a Supercritical Supersonic Inlet," *AIAA Journal*, Vol. 26, No. 11, 1988, pp. 1336–1345.

[18]Robinet, J. C., and Casalis, G., "Shock Oscillations in Diffuser Modeled by a Selective Noise Amplification," *AIAA Journal*, Vol. 37, No. **XX**, 1999, pp. 453–459.

[19]White, F. M., *Viscous Fluid Flow*, McGraw–Hill, New York, 1974.

[20]Rodi, W., "Experience with Two-Layer Models Combining the k–ε Model with a One-Equation Model Near the Wall," AIAA Paper 91-0216, Jan. 1991.

[21]Watson, W. R., and Myers, M. K., "Inflow–Outflow Boundary Conditions for Two-Dimensional Acoustic Waves in Channels with Flow," *AIAA Journal*, Vol. 29, No. **XX**, 1991, pp. 1383–1389.

[22]Roache, P. J., *Computational Fluid Dynamics*, Hermosa, Albuquerque, 1982, pp. 282–283.

[23]Harten, A., "High Resolution Schemes for Hypersonic Conservation Laws," *Journal of Computational Physics*, Vol. 49, No. 3, 1983, pp. 357–393.

[24]Yee, H. C., "A Class of High-Resolution Explicit and Implicit Shock-Capturing Methods," Lecture Series for Computational Fluid Dynamics, von Kármán Inst. for Fluid Dynamics, Rhode-St-Genese, Belgium, 1989; also NASA TM-101088, Feb. 1989.

[25]Oh, J. Y., "Numerical Study of Steady and Oscillatory Flow Structures in an Axisymmetric Supersonic Inlet," Ph.D. Dissertation, Dept. of Mechanical Engineering, Pennsylvania State Univ., University Park, PA, Aug. 1994.

[26]Taylor, G. I., and Maccoll, J. W., "The Air Pressure on a Cone Moving at High Speeds," *Proceedings of the Royal Society of London, Series A: Mathematical and Physical Sciences*, Vol. 139, No. 838, 1933, pp. 278–311.

[27]Spalart, P. R., "Direct Simulation of a Turbulent Boundary Layer up to $Re_\theta = 1410$," *Journal of Fluid Mechanics*, Vol. 187, 1988, pp. 61–98.

[28]Roache, P. J., "Quantification of Uncertainty in Computational Fluid Dynamics," *Annual Review of Fluid Mechanics*, Vol. 29, 1997, pp. 126–160.

[29]Green, J. E., "Interactions between Shock Waves and Turbulent Boundary Layers," *Progress in Aerospace Sciences*, Vol. 11, 1970, pp. 235–340.